



OPEN Efficient photovoltaics integrated with innovative Li-ion batteries for extreme (+ 80 °C to –105 °C) temperature operations

Ethan Adams¹, Alexander Camacho¹, Evan Mammana¹, Soohwan Kim¹, Thomas E. Adams² & Vilas G. Pol¹✉

Current pursuits for further exploration into extreme environments like aerospace, outer space, and Arctic conditions require matching energy harvesting and storage technologies that can efficiently operate in extreme conditions. While current systems utilize a variety of different battery chemistries, photovoltaics, and radioisotope power systems to power and store the required energy, at ultra-low temperatures (< -60 °C), current batteries have extremely low-capacity retention (< 20 %) and require extensive heating coils and thermal shielding to work when paired with photovoltaics. To simultaneously test both current and new types of whole photovoltaics (PV) and innovative Li-ion batteries (LIBs) at extreme temperatures (180 °C to -185 °C) in the research laboratory, an Integrated Photovoltaic and Battery (IntPB) system has been developed at Purdue University. The first IntPB allows for testing a variety of energy storage devices (Li-ion, Na-ion, K-ion batteries) and harvesting technologies (PV, radioisotope, thermoelectric), verifying their suitability when paired at a wide range of temperatures and charging protocols. A specially designed IntPB system allowed for testing either small-scale coin cells (10 mAh) or larger pouch cells (1 Ah) with polycrystalline silicon PV between 80 °C to -120 °C. It effectively charged the lithium metal battery using a niobium tungsten oxide cathode and 1 M LiFSI in cyclopentyl methyl ether electrolyte to comparable capacities. When discharged with the battery cycler, the battery provided similar capacities at a constant current discharge, thus ensuring that the system was able to charge/discharge equivalent amounts of energy. At 80 °C, -105 °C, and -120 °C, the IntPB was able to charge/discharge 150 mAh g⁻¹, 30 mAh g⁻¹, and 6 mAh g⁻¹ capacity, respectively. This indicated that the pairing of the PV and battery was able to charge/discharge the battery at a wide range of temperatures that the system would be expected to experience in places such as the desert, Arctic, or outer space. Contrasting temperature effects in integrated PV-battery systems pose a significant challenge: PV efficiency improves at low temperatures due to increased semiconductor band gap, while LIB performance deteriorates due to sluggish Li-ion movement within the electrolyte and across interfaces, necessitating careful system optimization to balance enhanced PV output with limited battery storage capacity.

An electrochemical battery that operates in extreme hot and cold temperatures would provide compelling solutions for defense and commercial applications and systems in space, Lunar, Arctic, Antarctic, and subsurface environments¹. In present systems used at ultra-low temperatures (ULT, < -60 °C), battery performance is limited by inherently poor ion (Li⁺) transport in the electrolyte. Thus, either temperature controls are added to warm the battery to improve conductivity or the battery is used as a backup or secondary energy storage source. Examples of these temperature management approaches can be found in numerous the National Aeronautics and Space Administration (NASA) orbiters and rovers^{2–5}. Orbiters can use their solar panels for the primary energy generation, with rechargeable batteries to store energy to provide power at night. The Mars Reconnaissance Orbiter is powered by two 32 V, 1000 W solar panel arrays which also charges two 32 V, 50 Ah) nickel-hydrogen batteries for continuous operation during the 2-hour day/night orbit. In 1996, the Sojourner rover went from initially using solar panels to a radioisotope power system (plutonium dioxide) to provide constant, steady state usage with lithium-ion batteries (LIBs) to meet peak demands^{6,7}. Rovers, such as Curiosity (2020), use a radioisotope thermoelectric generator using plutonium-238 as the main power, 110W_e and 1830W_t.

¹Davidson School of Chemical Engineering, Purdue University, West Lafayette, IN 47907, USA. ²Crane Division, Naval Surface Warfare Center, 300 Highway 361, Crane, IN 47522, USA. ✉email: vpol@purdue.edu

of waste heat, and two 28 V, 43 Ah LIBs for peak power demand⁶. Combinations of these systems has been used by NASA reliably for decades including the Apollo, Viking, Pioneer, Voyager, Ulysses, Galileo, Cassini, and New Horizons missions^{8,9}.

Despite the widespread use of solar panels or some alternative energy source coupled with batteries for energy storage, these systems all require extensive and complex thermal control and management designs in the form of radiators, surface coatings, insulation, and heaters. More practical testing utilizing cutting edge research to allow for scale-up and industrial use for energy generation and storage systems is critical to transition from laboratory research to a more applied focus. Commercially available test systems are either capable of cycling a photovoltaic (PV) cell or a battery separately at a range of temperatures, but not in a hybrid configuration with both being at low temperature (LT)^{10–12}. This is a particular problem as PVs' current and voltages have opposite trends as a function of temperature, with a decrease in temperature causing the PV's voltage to increase but its' current to decrease; these results and causes are explained in the following discussion section. Though commercial temperature chambers can go up to 100 °C, none can go down to -100 °C or lower. Therefore, to fully assess the performance of a PV and battery energy system at ULTs, a custom test system and fixture are required.

C. M. Jamison et al. developed a novel lithium-ion battery cyler capable of testing coin and pouch cells at ultralow temperatures down to -175 °C, simulating extreme conditions¹³ found in lunar and space missions. This system, called the extreme low-temperature system (ELTS), uses liquid nitrogen flow to achieve temperatures between -175 °C and 25 °C. The ELTS enables testing of $\text{Li}_4\text{Ti}_5\text{O}_{12}||\text{Li}$ cells with a specialized electrolyte¹⁴ at various low temperatures, demonstrating discharge capacities of 159.04, 119.12, 101.79, and 33.06 mAh g⁻¹ at room temperature, -20 °C, -40 °C, and -60 °C, respectively.

Notably, the system achieved a reversible capacity of 7.12 mAh g⁻¹ at -100 °C, marking the first such test at this extreme temperature. To observe the behavior of a PV and a novel LIB hybrid energy source at ULTs, a custom system named the *Integrated Photovoltaic and Battery* (IntPB) has been designed to safely cycle test individual energy generation and storage sources and hybrid energy sources at -100 °C as below. This work's motivation and end goals is depicted in Fig. 1, as it is our hope that the designed system will help enable new innovative technologies to be tested together at ULTs to rigorously test their performance with these improved systems eventually getting implemented in technologies like satellites and rovers. While results can be found for both the individual components' performance at these temperatures, no previously reported data exists to compare results. The IntPB was designed with flexibility to allow for individual testing of energy generation sources like PVs and nuclear batteries (betavoltaics) along with various energy storage technologies like LIBs (coin cell to small pouch cell), capacitors, and hybrid energy sources. The chamber was designed with electrical throughputs for data acquisition (voltage, current, and temperature), charging, discharging, and to tune the open-circuit PV voltage to match the maximum LIB voltage to prevent overcharging. This tuning circuit, located external to the PV/LIB source, allows the battery to fully charge at a specific temperature. When tested at a range of temperatures from 80 °C to -105 °C, the battery exhibited charge capacity values within 10% of the energy delivered by the PV. The charge capacity values were similar to ones measured when only the battery was tested. For these tests a commercially available polycrystalline silicon 5 V, 30 mA, PV was paired with a niobium tungsten oxide LIB ($\text{NbWO}||\text{Li}$); explanations on its reason and specifics are discussed below.

Designing integrated silicon photovoltaic cells with batteries for >-100 °C operation poses significant challenges due to contrasting temperature effects: while PV efficiency improves at low temperatures, LIB performance declines significantly¹⁵. At ULTs, LIBs experience sluggish Li-ion movement, increased internal resistance, and electrolyte limitations, leading to reduced capacity and power output¹⁶. Recent advancements

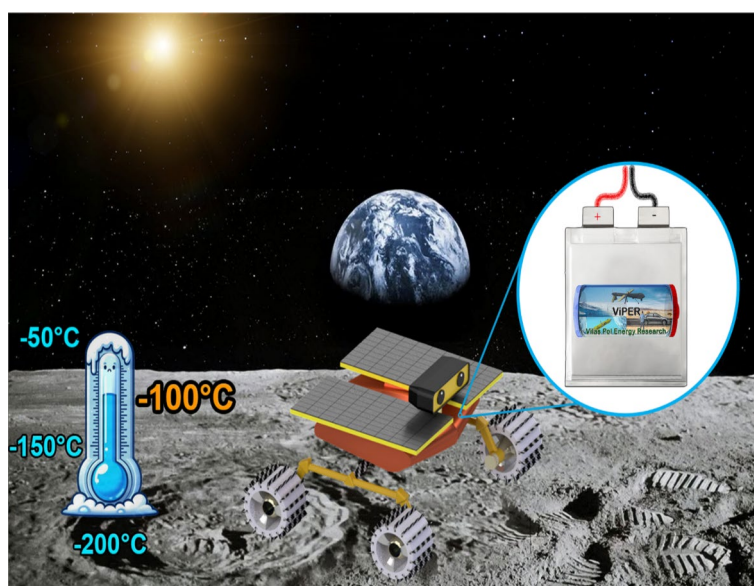


Fig. 1. Pictorial motivation and potential testing usage for integrated photovoltaic-Li-ion battery system.

in PV materials, including silicon-based, organic, and perovskite solar cells, have improved efficiency and stability, with perovskite cells achieving a record efficiency of 29.15 %, surpassing traditional crystalline silicon technology¹⁷.

Addressing these challenges requires innovative approaches in materials science, battery chemistry, and system design, such as LT manufacturing processes and novel interconnection techniques to reduce silver consumption and avoid lead-containing materials. The Integrated Photovoltaic and Battery (IntPB) system represents a significant advancement in testing hybrid energy sources for extreme environments, enabling simultaneous evaluation of photovoltaic cells and batteries at ULTs down to -100°C . Its flexible design accommodates various energy generation and storage technologies, while a unique voltage matching circuit optimizes performance across a wide temperature range. The IntPB demonstrates consistent performance from 80°C to -105°C , with battery charge capacity values within 10 % of the energy delivered by the PV, providing crucial data for developing energy systems for space exploration and other extreme applications.

Experimental setup for IntPB

The IntPB was designed for ultra-low temperatures and sized to hold a PV and a battery, either coin or pouch cell, with a glass window to allow for PV illumination with a light source. A small PV cell (polycrystalline silicon 5 V, 30 mA) was used and irradiated by a light source to determine the open circuit voltage (V_{OC}) and short-circuit current (I_{SC})⁵. A 9 W and 32 W LED grow light, which provide a light spectrum similar to that of the sun, were used to irradiate the when connected to a coin cell or to a pouch cell, respectively¹⁸. The test chamber was custom made by INSTEC per our design requirements. It is an aluminum clam shell with a glass window on top with the top and bottom parts being held together with 4 screws and a silicon gasket to allow for a hermetic seal to be formed. There are two sets of feedthrough ports, one for liquid nitrogen (LN_2) and the other for argon gas, with the Ar gas being critical to keeping the gas in the chamber free from water vapor and any ice crystals when the system is cooled. Eight electrical throughputs are provided for data acquisition measurements (voltage, current, and temperature), charging, discharging, and to tune the open-circuit PV voltage to match the maximum LIB voltage to prevent overcharging. The PV and LIB are positioned atop the platen that is temperature regulated with LN_2 or heating coils controlled by the INSTEC temperature controller. The setup of the custom INSTEC test chamber and temperature controller is shown in Fig. 2.

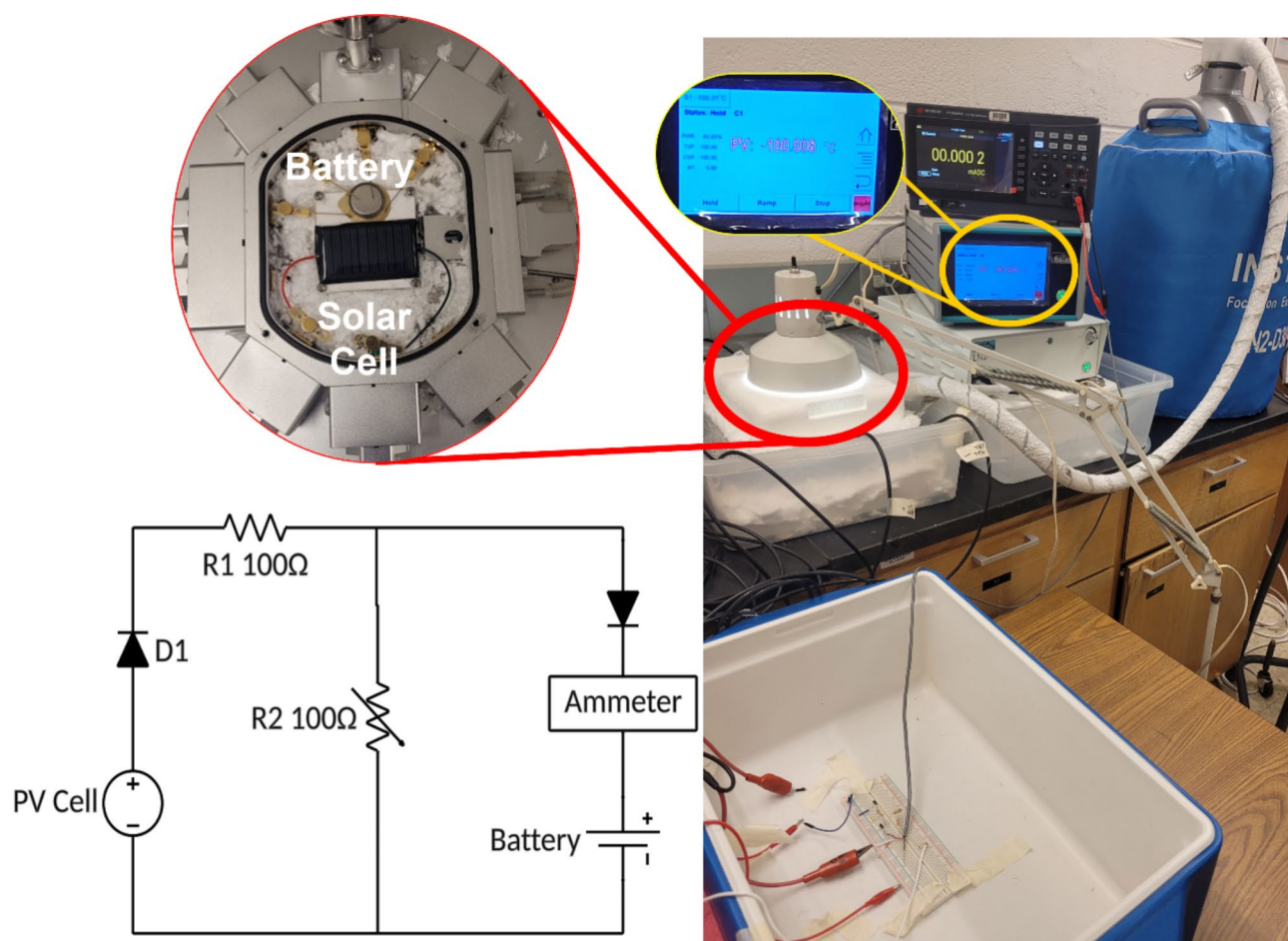


Fig. 2. Setup of Test Chamber, Temperature controller, and LN_2 connections.

The temperature of the test chamber is controlled by an INSTEC controller in line with the LN_2 cooling tubing before entering the test chamber. Inside the INSTEC chamber there is a stainless steel block, which the PV and LIB sit on top, that have channels bored into it, similar to a heat exchanger, allowing LN_2 to be pumped through it, directly cooling through conductive heat transfer. A proportional–integral–derivative controller regulates the temperature using feedback from a thermocouple that measures the stainless steel block's surface temperature by adjusting the LN_2 scroll pump's speed, the rate at which it pumps LN_2 from the 30 L dewar through the INSTEC. For ULTs, the test chamber's exterior was insulated in a box with FiberFrax to decrease the amount of heat transfer losses from its exterior while argon gas is pumped inside the sealed INSTEC chamber to prevent and water vapor from condensing and freezing on the cold surfaces of the stainless steel block, PV, and LIB.

To allow the LIB coin cell to be charged by the PV and discharged by an Arbin test channel, the setup shown in Fig. 3 was developed where a voltage divider circuit was used to adjust the open-circuit voltage of the PV to that of the LIB's maximum voltage. In the circuit, two Schottky diodes are used one connected after the positive terminal of the PV, D_1 , to prevent backflow of current during charging with the second one, D_2 , preventing the LIB from discharging through R_2 once the battery is fully charged. In reference to Eq. 1 a voltage divider is used to set the charging voltage to a value matching the LIB's cutoff voltage, ~ 3.0 V for $\text{NbWO}||\text{Li}$, through adjusting the ratio between R_1 and R_2 . A Schottky diode, specifically was chosen over other diodes due to its lower forward voltage drop which is kept at around 0.47 V for the entire range of charging currents used in this work. The value given in Eq. 1 is then used as an estimate, along with final testing/adjustments being made, with the battery still disconnected, to account for small variations in resistor accuracy and contact resistance inside the breadboard¹⁹.

$$V_{\text{Battery}} = (V_{\text{PV}} - V_{D1}) \left(\frac{R_2}{R_1 + R_2} \right) \quad (1)$$

Only the PV and LIB are placed in the test chamber, the other components are externally connected by the electrical throughput ports. To mitigate noise in measurements, all test and monitoring leads were shielded and grounded to a single Earth-ground point. A digital ammeter is connected between the diode D_2 and the positive terminal of the LIB to measure current for calculating capacity. Initial setup had unshielded wires without a common ground, yielding fluctuating amperage readings as shown in Figure S1. To monitor the LIB's voltage, as shown in the zoomed in image of Fig. 2, the LIB was connected with four leads, two of each for the positive

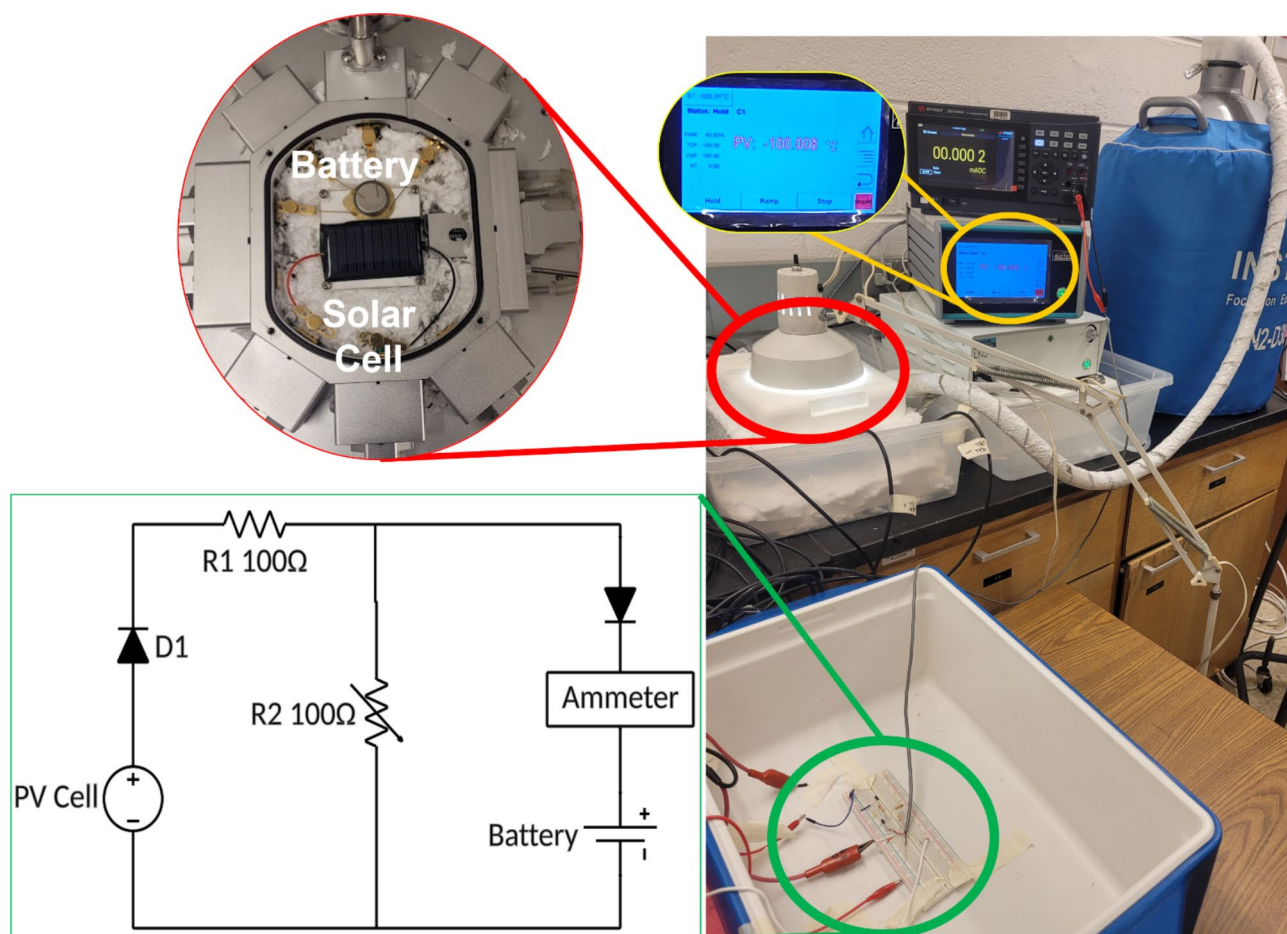


Fig. 3. PV/LIB hybrid interface circuit.

and negative terminals of the LIB. One pair (1 positive and 1 negative) are used for the regular pass through of current for the charging circuit, while the other pair is used to monitor the voltage of the battery in real time using a separate Arbin galvanostatic battery cycler that can record the LIB's voltage without affecting the charging of the battery. All circuitry except for the ammeter and the PV/LIB, are contained on the breadboard in Fig. 3. The operation of the PV/LIB hybrid source was assessed in this fashion. PV and discharged LIB was placed on the INSTEC chamber plate and connected. Chamber was secured and connected to LN₂ and Ar. Then the LIB was connected to an Arbin cycler channel and to the breadboard components. The light source was then turned on to illuminate the PV with the digital ammeter measuring the charging current and the Arbin cycler monitoring the LIB's voltage. This was left on until the LIB's voltage had reached its cutoff voltage and the charging current had decreased to ~ 1/30 of its initial value.

Once the LIB is fully charged, the LIB is manually disconnected from the charging circuit by detaching the positive and negative cables that connect the INSTEC probes to the breadboard. The battery is then discharged through the Arbin galvanostatic battery cycler at a constant current roughly equivalent to the average charge current that the battery experienced during charging. The discharge capacity can then be compared to its charge capacity to show that the system works for both charging and discharging at ULT. For future work, the Arbin battery cycler enables the discharge procedure to be customizable to match a desired load curve that actual systems would pull over time so that systems could be directly tested on their ability to power their desired applications.

Characterization of photovoltaic cell

Since the cutoff voltage of the chosen LIB (NbWO₃||Li) is 3.0 V, a 5 V PV was selected to account for roughly 2 V of additional drop across the diodes and resistors. However, as the PV's voltage and current vary as a function of temperature, these values need to be gathered so that a proper R₁ and R₂ can be chosen at each temperature to ensure that the charging voltage the battery experiences is kept constant at ~ 3 V. To determine these values, the PV was disconnected from the charging circuit and replaced with a Gamry potentiostat with the photon flux kept constant via holding the light source at a constant distance and luminosity throughout the experiment. At each temperature the PV's current response to an applied electrical potential that is swept between -0.5 V and a potential 0.3 V above the PV's V_{OC}, the PV's potential when it is measured without a load is shown in Fig. 2a as the Light IV curves.

Typically, PV cells generate electricity more effectively at lower temperatures for the same amount of sunlight because of (i) the increased bandgap energy (electron potential between electrons in the valence band and holes in the conduction band is increased) in the silicon semiconductors, (ii) enhanced mobility of charge carriers (electrons and holes have reduced recombination rate and phonon scattering), and (iii) larger increase in effective voltage than its subsequent decrease in current leads to a larger max power and fill factor (FF).

In Fig. 4a, the PV's light curves depict the voltage and current operating values of the polycrystalline silicon PV at temperatures 30 °C apart between 80 °C and -130 °C, with the y-intercept representing the maximum possible current, I_{SC}, and the maximum possible voltage, V_{OC}. For PN junction SCs, as temperature increases its I_{SC} increases while its V_{OC} decreases with this relationship being reversed as temperature decreases. At increased temperatures, the amplitude of a bond's vibration is increased causing for an effective larger interatomic spacing which results in the band gap for a material decreasing. The band gap is affected by the interatomic spacing as when the distance between atoms increases the potential seen by the electrons in this material decreases which results in a decrease of the band gap at elevated temperatures^{20,21}. From Fig. 4a this results in the V_{OC} increasing from 4.1 V to 7.3 V and the I_{SC} decreasing from 2.84 mA to 2.69 mA between 80 °C to -130 °C. Increased temperature also results in an increase in the carrier, *electron-hole pair*, concentration causing for an increase in the amounts of photocurrents produced at elevated temperatures. This effect also causes PV's dark current, the current generated from the diffusion of minority carriers to recombination sites, to increase due to the strong temperature dependence for this current. The dark current (Fig. 4b) is affected by three main factors the temperature, diffusivity of the minority carriers, and the lifetime of the minority carrier with the two properties other than temperature being more affected by the specific material chosen in the PV²². This relation can be expressed in Eq. 1, where the dark current (j_o) is written in terms of the material properties and temperature:

$$j_o = \left[4 \left(\frac{2\pi m_e}{h^2} \right)^3 \right] \left[\frac{\mu_h \mu_e}{L_h \sigma_e} \right] \left[\left(\frac{kT}{e} \right)^4 \exp \left(-\frac{eV_g}{kT} \right) \right] \quad (1)$$

In Eq. 1 the terms to the left of the temperature expressions are constants, found from the specific material properties that have only minor correlations with temperature, so an increase in temperature causes a rise in the dark current. While this leads to an overall increase in the net current from the PV, j_s, the ratio of j_s to j_o decreases for a given illumination intensity^{22,23}. This is important as this decrease is what results in the PV's V_{OC} decreasing with an increase in temperature as described in Eq. 2²²:

$$V_{OC} = j_s \frac{kT}{e} \ln \left(1 + \frac{j_s}{j_o} \right) \quad (2)$$

When different trends from this equation are analyzed due to the small increase in total current, j_s, compared to the more significant decrease in the ratio of total current to dark current this results in a net decrease in V_{OC} as temperature increases. This is shown in Fig. 4a as the temperature has a greater effect on the PV's V_{OC} than on its I_{SC}, with the I_{SC} increasing by only 0.05 mA from -130 to 20 °C. Generally, the I_{SC} is more affected by the ability of the PV to trap light and utilize longer wavelengths of light rather than its E_g. For the V_{OC} there was a larger, roughly linear increase of V_{OC} with decrease in temperatures as it increased from 5.1 V at 20 °C to 7.25 V at -130

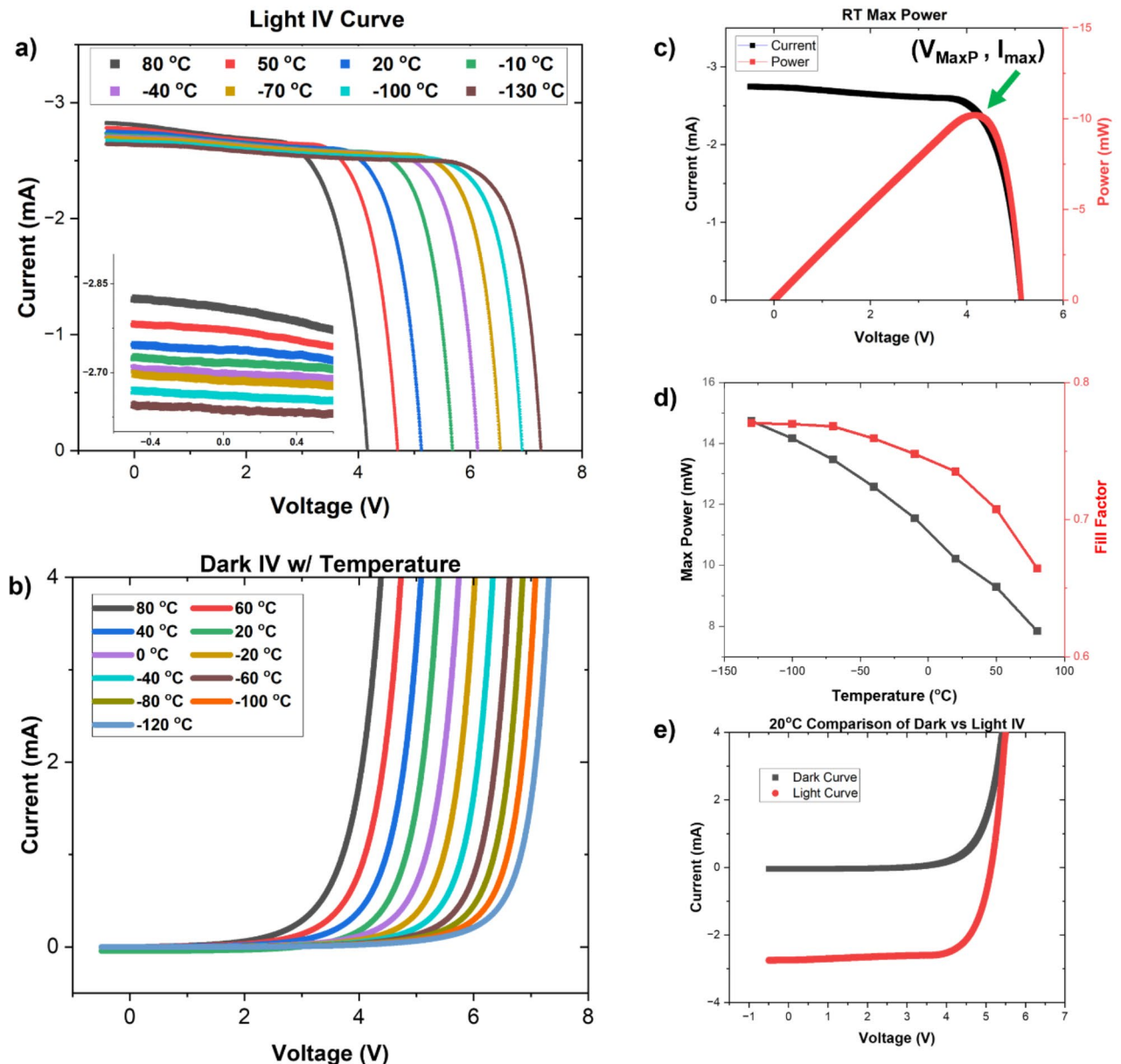


Fig. 4. Photovoltaic's: (a) Light IV curves measured between 80 °C to -120 °C; (b) Dark IV V_{OC} and current as a function of temperature; (c) Max Power curve at 20 °C; (d) Max power and fill factor as a function of temperature; (e) Single temperature comparison of light and dark IV curves.

°C. The V_{OC} and I_{PV} give bounds that the PV has to operate at a given temperature. From this data, the optimal operating potential can be determined in Fig. 4c where at the 20 °C the light IV curve along with its' power curve ($P=IV$), is plotted to determine the PV's best operating conditions (V_{MaxP} , I_{Max}) that leads to maximum net power. Figure 4d plots the PV's maximum power as a function of temperature along with its resulting FF, values determined in Eq. 3.

$$Fill\ Factor\ (FF) = \frac{V_{MaxP} * I_{Max}}{V_{OC} * I_{SC}} \quad (3)$$

The FF represents the ratio of the maximum power to the product of its maximum voltage and current, with a value close to 1 representing that the curve approximates a square. Figure 4d shows that as temperatures decrease both the maximum power and FF increase with the largest values being generated at -130 °C. However, interestingly while the PV's power curve follows an approximately linear increase with decreasing temperature the FF begins to plateau around -70 °C with it approaching an asymptote of 0.77 at -130 °C. Figure 4e shows that the PV is working properly as at higher voltages above the V_{OC} the two curves overlap a phenomenon which is

expected due to the light IV curves being a superposition of the natural ‘dark’ currents that are produced in the PV along with the current produced when light is applied to the PV. As the current generated with light is applied shifts the current to the 4th quadrant, at voltages above the V_{OC} the two curves should gradually overlay again²⁴.

Overall, this means that the PVs exhibit a higher efficiency at lower temperatures due to it minimizing thermal losses while enhancing the PV’s energy conversion. At lower temperatures less of the light is converted to heat while the charge mobility of its electrons and holes is increased, more efficient, due to the decrease number of charge carriers leading to less scattering from the various collisions between charge carriers^{25–27}. When combined with the reduced lattice vibrations along with increased band gap at decreased temperatures this results in increased carrier lifetimes, resulting in a larger V_{OC} , lower I_{SC} and an increased maximum power.

Characterization of PV-LIB hybrid energy source

Coin cells were made with Li-metal anodes, NbWO cathodes and an electrolyte using 1 M LiFSI in cyclopentyl methyl ether (CPME) were chosen¹³. This electrochemistry was specifically designed for ULTs. The electrolyte’s low freezing point ($-140\text{ }^{\circ}\text{C}$) and low desolvation energy allows for enhanced bulk and interfacial Li^+ transport when compared to other typical electrolytes¹³. The NbWO cathode’s rapid Li^+ diffusion allows the cell to cycle at temperatures below $-60\text{ }^{\circ}\text{C}$. Typical electrode materials like graphite, lithium iron phosphate, and lithium nickel manganese cobalt oxide have sluggish Li^+ kinetics for solid-state diffusion during the intercalation/de-intercalation process at LTs that create large overpotentials inside the cell resulting in very low-capacity retention and rate capability at these temperatures¹³. The chosen electrode material for this work, NbWO, is a type of pseudocapacitive charge storer as it enables Li^+ to be rapidly stored on the surface through surface-controlled reactions, along with enhanced solid-state transport through its open framework and large pentagonal channels. This combined system was shown to have superior ULT capability, allowing for up to 75 mAh g^{-1} at $-100\text{ }^{\circ}\text{C}$ ¹³.

Before charging the LIB at a given temperature the PV’s V_{OC} was used to calculate the necessary $R_{1,2}$. With the current charging circuit, the cells are charged at a constant voltage, meaning that the charging voltage is kept fixed at the battery’s cutoff voltage with the battery’s voltage slowly increasing along with its state of charge. This configuration results in the highest current to the battery being delivered initially with this current fading as the battery’s voltage approaches its cutoff voltage before decreasing to $\sim 0\text{ A}$ at longer durations as the internal resistance inside the battery prevents further charging²⁸. To ensure that the cell was not shorted by delivering too high a current, the initial current could be decreased by decreasing the photon flux from the light source along with increasing the values of R_1 and R_2 , while keeping the ratio constant, to ensure that the initial current didn’t exceed $C/2$ for the battery. The type of charging protocol approximates a trickle charge, so at decreasing temperatures the time needed to fully charge the battery increases. In Fig. 5a–e the time needed to charge the battery increases from 11 h at $80\text{ }^{\circ}\text{C}$ to 44 h at $-105\text{ }^{\circ}\text{C}$. Though not desired for this testing, the system could be modified to allow for a quicker charge, but this would require integrated circuitry and a controller that could more accurately control the current to match other charging protocols like with a constant current charge.

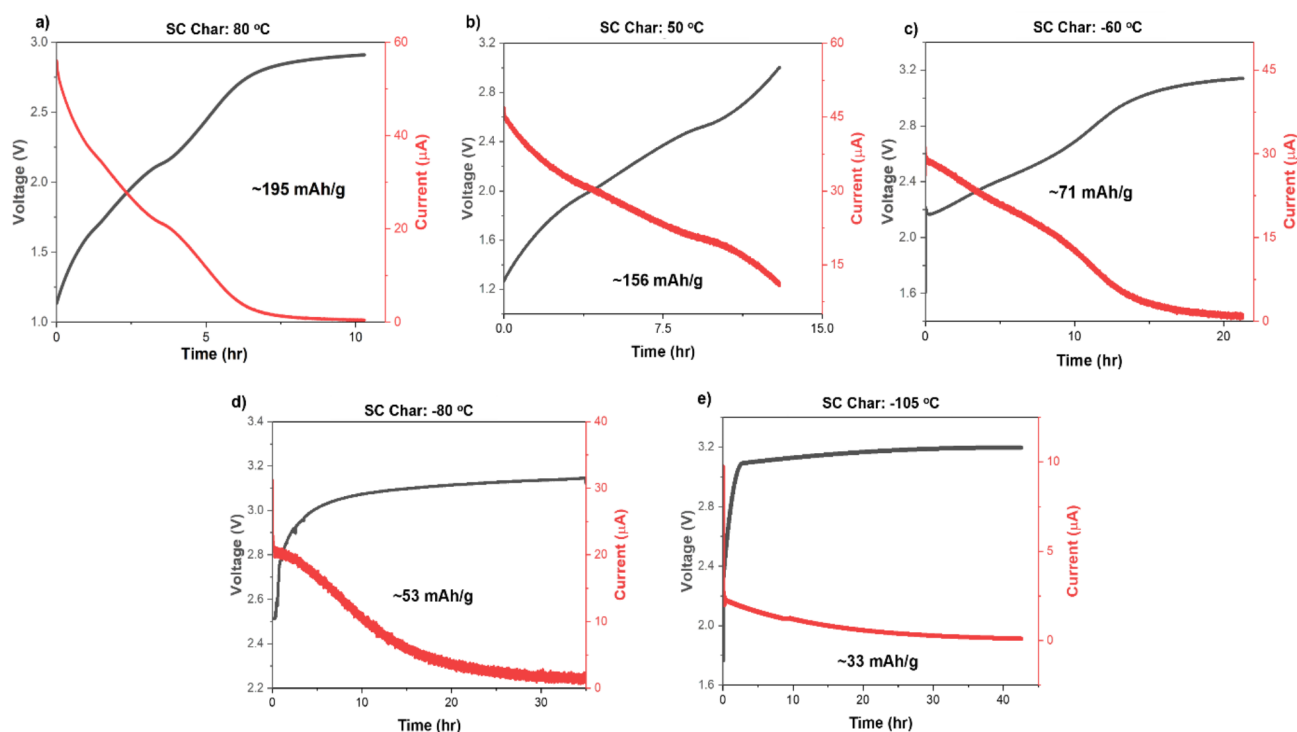


Fig. 5. Galvanostatic charge of the IntPB: (a–e) Charging of the prepared NbWO||Li cell at constant voltage at 80, 50, -60, -80, -105 °C.

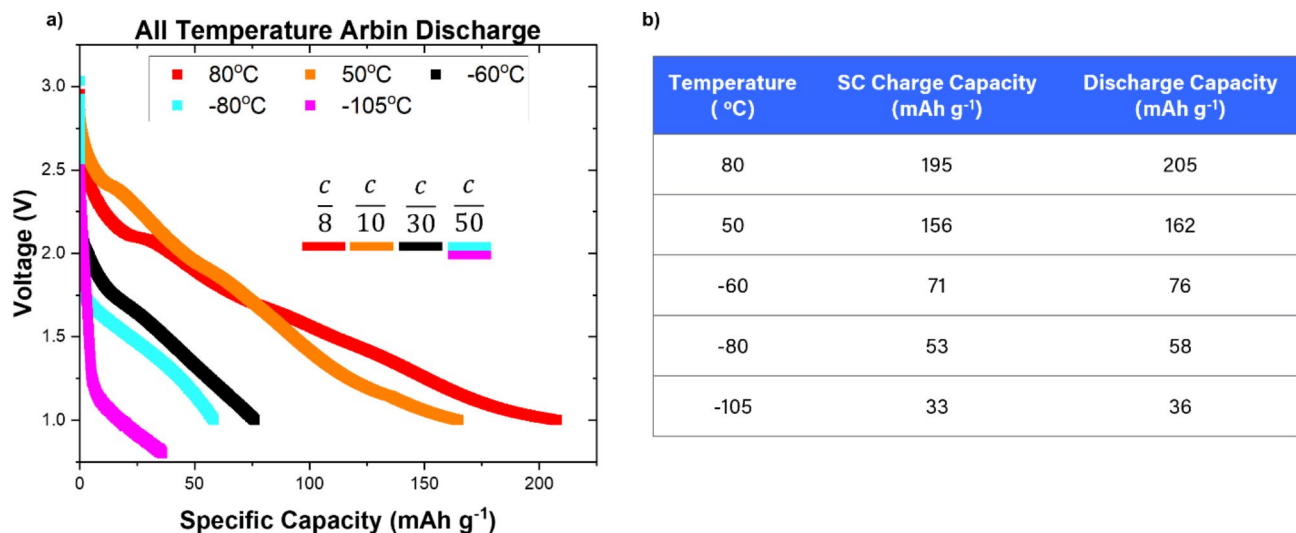


Fig. 6. (a) Galvanostatic discharge of the LIB through the Arbin cyclers at 80, 50, -60, -80, -105 °C; (b) Tabulated charge and discharge capacities at each temperature.

Figure 6a show the same cell being discharged directly after its charge at a constant current. At all temperatures the charge and discharge capacities were within 5–10 % with this difference mainly arising from the different charging/discharging procedures. The capacity values are tabulated in Fig. 6b. This provides evidence that the combination of PV and LIBs is a viable alternative to pre-existing technology for energy storage/generation at ultra-low temperatures. At all tested temperatures, an approximately 8 % difference between the energy input versus energy output indicated minimal energy loss. In addition to these results in Figure S2 additional charging/discharging data was gathered at -120 °C which had minimal capacity of around 6 mAh g⁻¹. In recent publication, Gouder and Lotsch discusses the integration of photovoltaic cells²⁹ with energy storage systems, highlighting the performance evaluations of solar batteries under varying conditions. It emphasizes the significance of simultaneous energy conversion and storage, which is essential for real-world applications, particularly in extreme environments. The study provides insights into the performance of these integrated systems at lower temperatures, enhancing their applicability in decentralized energy storage solutions.

Conclusion

A combined IntPB for testing the efficiency of storing and discharging capacity at various temperatures has been presented. The apparatus is easily modifiable to fit a variety of energy storage solutions and size demands, is low-cost, and is the first fully combined system that allows for both the PV and the LIB to be tested at the same temperature within a range of -180 °C to 300 °C. This system will allow for integrated testing of PVs and energy storage solutions like LIBs to be evaluated at their actual operating temperatures rather than only at room temperature. These tests are critical for understanding their applicability and fully testing their performance at extreme temperatures when deployed in Arctic or outer space conditions. Currently, the IntPB has allowed for a novel cell chemistry designed for ULTs to be charged at a wide range of temperatures from 80 °C to -105 °C before being discharged at the same temperature. This setup allows for reliable testing as the charge and discharge capacities of the battery are within 5 % of each other. The apparatus will be used to conduct further experiments into the combination of more novel energy generation and storage technologies at various temperatures by replacing the PV with other more experimental solar cells like perovskite-based PVs or betavoltaic cells and alternative chemistries for the LIB. Along with testing alternative energy generation technologies, this system will also be used to rigorously test the system's capability of meeting exact load and power demands at various temperatures.

Experimental Section/Methods

Electrolyte Preparation 1 M LiFSI in CPME electrolyte was prepared by dissolving LiFSI (187.1 mg) in CPME (1 mL) under argon atmosphere. Both materials were sourced from Sigma Aldrich.

Electrode Materials: NbWO material were synthesized using a thermal solid-state reaction of NbO₂ (Alfa Aesar) and WO₂ (Alfa Aesar). Before thermal treatment both precursors were thoroughly mixed to ensure homogeneity at the proper stoichiometric ratio (18:16) before being pressed into a pellet. This pellet was then heated inside a crucible at 1200 °C for 24 h in an air atmosphere to obtain the final product, NbWO.

Electrochemical characterization CR2032 half-cells were assembled in an argon-filled glovebox using NbWO electrodes, lithium metal foil (150 µm thick), Celgard 2500 polypropylene separator, and 1 M LiFSI in CPME electrolyte. The cells were cycled between 1.0 and 3.0 V vs. Li/Li⁺ using an Arbin BT2000 cyclers with Phoenix leads connected to a customized cooling plate.

PV materials The PVs used to charge the Li||NbWO coin cells were manufactured by Aoshike, 5 V 30 mA 53 mm x 30 mm mini solar panels. These PVs were irradiated with a GE 9 W LED grow light with reGrow Light LED Indoor Flood Light Bulb, Balanced Light Spectrum.

Data availability

A data availability statement: All data generated or analyzed during this study are included in this published article and its supplementary information files. The datasets used and/or analyzed during the current study available from the corresponding author on reasonable request.

Received: 22 October 2024; Accepted: 16 December 2024

Published online: 25 March 2025

References

- Gupta, A. & Manthiram, A. Designing Advanced Lithium-Based Batteries for Low-Temperature Conditions. *Adv. Energy Mater.* **10**, 1–14. <https://doi.org/10.1002/aenm.202001972> (2020).
- Mckissock, B., Loyselle, P. & Vogel, E. Guidelines on Lithium-ion Battery Use in Space Applications. Accessed: May 29, 2024. [Online]. Available: (2009). <http://www.sti.nasa.gov>
- Krause, F. C. et al. High Specific Energy Lithium Primary Batteries as Power Sources for Deep Space Exploration. *J. Electrochem. Soc.* **165** (10), A2312–A2320. <https://doi.org/10.1149/2.1061810JES/XML> (2018).
- Walker, W., Yayathi, S., Shaw, J. & Ardebili, H. Thermo-Electrochemical Evaluation of Lithium-Ion Batteries for Space Applications. *J. Power Sources* **298**, 217–227. <https://doi.org/10.1016/j.jpowsour.2015.08.054> (2015).
- Marsh, R. A. et al. Jul., Li Ion Batteries for Aerospace Applications, *J. Power Sources* **97–98**, 25–27. [https://doi.org/10.1016/S0378-7753\(01\)00584-5](https://doi.org/10.1016/S0378-7753(01)00584-5) (2001).
- Lyons, V. J. & Scott, J. H. An Overview of Space Power Systems for NASA Missions, in *Collection of Technical Papers – 5th International Energy Conversion Engineering Conference*, American Institute of Aeronautics and Astronautics Inc. pp. 298–313 <https://doi.org/10.2514/6.2007-4734> (2007).
- Borthomieu, Y. & Bernard, P. SECONDARY BATTERIES – NICKEL SYSTEMS | Nickel–Hydrogen, *Encyclopedia of Electrochemical Power Sources*. pp. 482–493. <https://doi.org/10.1016/B978-044552745-5.00157-X> (2009).
- Khan, J. & Arsalan, M. H. Solar Power Technologies for Sustainable Electricity Generation - A Review, *Renewable and Sustainable Energy Reviews*. **55**, 414–425. <https://doi.org/10.1016/j.rser.2015.10.135> (2016).
- Khan, Z., Vranis, A., Zavoico, A., Freid, S. & Mannes, B. Power System Concepts for the Lunar Outpost: A Review of the Power Generation, Energy Storage, Power Management and Distribution (PMAD) System Requirements and Potential Technologies for Development of the Lunar Outpost, in *AIP Conference Proceedings*, 1083–1092. <https://doi.org/10.1063/1.2169289> (2006).
- Hayat, M. B., Ali, D., Monyake, K. C., Alagha, L. & Ahmed, N. Solar energy—A Look into Power Generation, Challenges, and a Solar-Powered Future, *International Journal of Energy Research*, vol. 43, no. 3. John Wiley and Sons Ltd, pp. 1049–1067. <https://doi.org/10.1002/er.4252> (2019).
- Gurung, A. & Qiao, Q. Solar Charging Batteries: Advances, Challenges, and Opportunities, *Joule* 21217–1230. <https://doi.org/10.1016/j.joule.2018.04.006> (2018).
- Kin, L. C. et al. Efficient area matched converter aided Solar Charging of Lithium Ion Batteries Using High Voltage Perovskite Solar Cells. *ACS Appl. Energy Mater.* **3** (1), 431–439. <https://doi.org/10.1021/acsaem.9b01672> (2020).
- Jamison, C. M., Kim, S., Ramasamy, H. V., Adams, T. E. & Pol, V. G. Lithium-ion Battery Testing Capable of Simulating ‘Ultralow’ Lunar Temperatures. *Energy Technol.* 2200799. <https://onlinelibrary.wiley.com/doi/10.1002/ente.202200799> (2022).
- Ramasamy, H. V., Kim, S., Adams, E., Rao, H. & Pol, V. G. A Novel Cyclopentyl Methyl Ether Electrolyte Solvent with a Unique Solvation Structure for Subzero (–40°C) Lithium-Ion Batteries. *Chem. Commun.* **58**, 5124. <https://doi.org/10.1039/D2CC00188H> (2022).
- Shaker, L. M. et al. Examining the Influence of Thermal Effects on Solar Cells: A Comprehensive Review. *Sustainable Energy Res.* **11**, 6. <https://doi.org/10.1186/s40807-024-00100-8> (2024).
- Luo, H. et al. Lithium-Ion Batteries under Low-Temperature Environment: Challenges and Prospects. *Materials* **15**, 8166. <https://doi.org/10.3390/ma15228166> (2022).
- Machin, A. & Márquez, F. Advancements in Photovoltaic Cell Materials: Silicon, Organic, and Perovskite Solar cells. *Mater.* **17**, 5. <https://doi.org/10.3390/ma17051165> (2024).
- Morrow, R. C. LED lighting in horticulture. *HortScience* **43** (7), 1947–1950. <https://doi.org/10.21273/HORTSCI.43.7.1947> (2008).
- Nilsson, J. & Reidel, S. *Electric Circuits* 11th edn (Pearson, 2018).
- Sun, C., Zou, Y., Qin, C., Zhang, B. & Wu, X. Temperature effect of photovoltaic cells: a review, *Advanced Composites and Hybrid Materials*, vol. 5, no. 4. Springer Science and Business Media B.V., pp. 2675–2699, Dec. 01, doi: (2022). <https://doi.org/10.1007/s42114-022-00533-z>
- Chakraborty, P. K. & Mondal, B. N. A Note on Anomalous Band-Gap Variations in Semiconductors with Temperature. *Indian J. Phys.* **92**, 303–306. <https://doi.org/10.1007/s12648-017-1102-3> (2018).
- Decher, R. *Direct Energy Conversion: Fundamentals of Electric Power Production* (Oxford University Press, Inc, 1997).
- Angrist, S. *Direct Energy Conversion* 4th edn (Allyn and Bacon, Inc, 1982).
- University of Michigan–Dearborn, Vehicular Technology Society., IEEE Power Electronics Society., and Institute of Electrical and Electronics Engineers., 5th International IEEE Vehicle Power and Propulsion Conference: September 7–11., Dearborn, Michigan, USA. 2009. (2009).
- Hamzelui, N. et al. Aug., Toward the Integration of a Silicon/Graphite Anode-Based Lithium-Ion Battery in Photovoltaic Charging Battery Systems, *ACS Omega* 7(31), 27532–27541. <https://doi.org/10.1021/acsomega.2c02940> (2022).
- Üçtuğ, F. G. & Azapagic, A. Environmental Impacts of Small-Scale Hybrid Energy Systems: Coupling Solar Photovoltaics and Lithium-Ion Batteries. *Sci. Total Environ.* **643**, 1579–1589. <https://doi.org/10.1016/j.scitotenv.2018.06.290> (2018).
- Asrori, A., Rohman, F., Faizal, E. & Karis, M. The Design and Performance Investigation of Solar E-Bike using Flexible Solar Panel by Different Battery Charging Controller. *Int. J. Mech. Prod. Eng. Res. Dev.* **10** (3), 14431–14442. <https://doi.org/10.24247/ijmperdjun20201374> (2020).
- Gurung, A. et al. Highly Efficient Perovskite Solar Cell Photocharging of Lithium Ion Battery using DC–DC Booster. *Adv. Energy Mater.* **7** (11). <https://doi.org/10.1002/aenm.201602105> (2017).
- Gouder, A. & Lotsch, B. V. Integrated Solar batteries: Design and Device Concepts. *ACS Energy Lett.* **8** (8), 3343–3355. <https://doi.org/10.1021/acsenenergylett.3c00671> (2023).

Acknowledgements

We would like to acknowledge the help of Ryan Gallagher for his help in testing out various circuit designs for the chosen charging circuit and Jamee Boyer for his help in collecting some of the ultra-low temperature data.

Author contributions

Ethan Adams carried out most of the research activities under the guidance of Dr. Pol. Alexander Camacho, Evan Mammana, Soohwan Kim assisted than on various stages of the project for completion. Thomas Adams helped on integrating the solar and battery systems.

Declarations

Competing interests

The authors declare no competing interests.

Additional information

Supplementary Information The online version contains supplementary material available at <https://doi.org/10.1038/s41598-024-83673-0>.

Correspondence and requests for materials should be addressed to V.G.P.

Reprints and permissions information is available at www.nature.com/reprints.

Publisher's note Springer Nature remains neutral with regard to jurisdictional claims in published maps and institutional affiliations.

Open Access This article is licensed under a Creative Commons Attribution-NonCommercial-NoDerivatives 4.0 International License, which permits any non-commercial use, sharing, distribution and reproduction in any medium or format, as long as you give appropriate credit to the original author(s) and the source, provide a link to the Creative Commons licence, and indicate if you modified the licensed material. You do not have permission under this licence to share adapted material derived from this article or parts of it. The images or other third party material in this article are included in the article's Creative Commons licence, unless indicated otherwise in a credit line to the material. If material is not included in the article's Creative Commons licence and your intended use is not permitted by statutory regulation or exceeds the permitted use, you will need to obtain permission directly from the copyright holder. To view a copy of this licence, visit <http://creativecommons.org/licenses/by-nc-nd/4.0/>.

© The Author(s) 2025